

and where $K(\beta_0)$ is given by Eq. (A9). When $\gamma \neq 1$, both β_0 and the slope $K(\beta_0)$ are most easily obtained numerically from a plot of Eq. (A6). In the present Ar⁺-Ar case, where $\gamma = 1$ and $\beta_0 = \pi/2$, one finds $f(\pi/2) = 0$ and $K(\pi/2) = T_0 \sin 2\theta$. Thus, Eq. (C2) reduces to

$$\beta_0 - \beta = 2\epsilon_x / \sin 2\theta, \quad (\text{C4})$$

for $\gamma = 1$.

The next step is to relate ϵ_x to the temperature t . The number of target particles dN having x momentum in the range $d\epsilon_x$ is given by

$$dN/d\epsilon_x = (\text{const}) \exp[-\epsilon_x^2 T_0 / kt], \quad (\text{C5})$$

where k is Boltzmann's constant. Equation (C4) shows that $\beta_0 - \beta$ is proportional to ϵ_x so that the line shape will be Gaussian as in Eq. (C5). The $1/e$ height in Eq. (C5) occurs at a particular value ϵ_x' where the exponent has unit magnitude. Thus

$$\epsilon_x' = (kt/T_0)^{1/2}. \quad (\text{C6})$$

Using Eq. (C4) one finds that the corresponding half-

width $\delta\beta_t$ is given by

$$\delta\beta_t = 2\epsilon_x' / \sin 2\theta = 2(kt)^{1/2} / (T_0^{1/2} \sin 2\theta). \quad (\text{C7})$$

The relationship between Q and β is linear in the region of β_0 , and there is a half-width δQ_t of the distribution in Q corresponding to $\delta\beta_t$. Thus, using Eq. (5),

$$\delta Q_t = \delta\beta_t T_0 \sin 2\theta. \quad (\text{C8})$$

When this is combined with Eq. (C7) there is an extremely simple result:

$$\begin{aligned} \delta Q_t &= 2(T_0 kt)^{1/2} \\ &= (0.010) T_0^{1/2}. \end{aligned} \quad (\text{C9})$$

The numerical factor, 0.010, is to be used when both δQ_t and T_0 are in keV and when t is room temperature, or 300°K. A thermal half-width (at $1/e$ height) δQ_t of 0.072 keV is predicted at $T_0 = 50$ keV and 0.023 keV at $T_0 = 5$ keV. Neither of these widths is negligible at the energies in question. There would be some advantage if the gas target region were at low temperature, since these half-widths, as seen in Eq. (C9), scale as the square root of the temperature.

Statistical Model for the Ar⁺-on-Ar Collision*

EDGAR EVERHART AND QUENTIN C. KESSEL

Physics Department, The University of Connecticut, Storrs, Connecticut

(Received 23 November 1965; revised manuscript received 1 March 1966)

This paper introduces a model to describe and predict the preceding experimental results on Ar⁺-Ar scattering. In considering a number of collisions in a data set it is assumed that there is a distribution among the inelastic energies of the atoms after the collision. It is further assumed that the energy received by one atom is not correlated with the energy received by the other atom in the same collision. The model, whose distribution widths are fitted to the data, predicts the average inelastic energy loss \bar{Q}_{mn} associated with a collision which results in one atom becoming m times ionized and the other n times ionized. The relative abundance \bar{p}_{mn} of the (m, n) reaction is also predicted. The values of \bar{Q}_{mn} and \bar{p}_{mn} so predicted agree well with the data. The model allows derivation from the data of the probability P_i that an atom, which received a particular inelastic energy E , subsequently becomes i times ionized. These derived $P_i(E)$ curves are rather similar in form to those which have been calculated by Russek. Under some circumstances there is a triply peaked structure to the inelastic energies transferred in these collisions. This structure is explained within the framework of the present model. Indirect evidence is presented that in the more violent collisions there may be one fast electron emitted per atom whose kinetic energy is a sizeable fraction of the inelastic energy.

1. INTRODUCTION

THE coincidence measurements of Ar⁺-Ar collisions of the preceding paper¹ are presented in a way so as to be independent of the model used to describe the collision. In the present paper we analyze and correlate these data. The model presented here is a

further development along the lines of our recent letters.^{2,3}

Starting with the concepts of the Russek⁴ theory of statistical distribution of energy to the several electrons on an atom, our model includes also the effect of sta-

* This study was supported by the U. S. Air Force Office of Scientific Research.

¹ Q. C. Kessel and E. Everhart, preceding paper, Phys. Rev. **146**, 16 (1966).

² E. Everhart and Q. C. Kessel, Phys. Rev. Letters **14**, 247 (1965).

³ Q. C. Kessel, A. Russek, and E. Everhart, Phys. Rev. Letters **14**, 484 (1965).

⁴ A. Russek and M. T. Thomas, Phys. Rev. **109**, 2015 (1958); **114**, 1538 (1959); J. B. Bulman and A. Russek, *ibid.* **122**, 506 (1961); A. Russek, *ibid.* **132**, 246 (1963).

tistical distribution of inelastic energy among the many atoms comprising a data set. Instead of using Russek's computed ionization probabilities, we determine these quantities by analysis of the data. Recently, Fano and Lichten⁵ suggested a "promotion" mechanism for accounting for the observed structure in the inelastic energy. They predicted that there should be one or two high-energy electrons released in some of these collisions, and at first glance it appeared that their description was in opposition to Russek's concepts. However, it is shown here that the data are best described by a model which combines parts of these two descriptions.

Besides the data of the preceding paper, there are the experiments of Afrosimov, Gordeev, Panov, and Fedorenko⁶ whose results on Ar^+-Ar agree well with ours where there is common data, as seen in Fig. 8 of the preceding paper.¹ They have interpreted the observed structure in terms of characteristic *excess* energy losses R^* (the inelastic energy loss for a particular reaction minus the corresponding spectroscopic ionization-energy deficit). The R^* values are attributed to levels of collective electronic oscillations existing during the collision. This concept is further developed by Amusia.⁷ However, it will be shown here that the R^* concept does not fit all the data now available on Ar^+-Ar collisions.

There is the recent statement by Afrosimov *et al.*,⁸ that there are characteristic structures to the inelastic energy-loss values which depend on the collision combination. They found in studying Ar^+-Ar , Ne^+-Ar , and Ne^+-Ne that each combination has a characteristic structure, but that Ne^+-Ar structure could not be predicted simply from Ar^+-Ar and Ne^+-Ne data. Despite the fact that we reject the R^* concept as presented⁶⁻⁸ the above measurements of structure are yet consistent with the new interpretation and model presented here. The distinction must carefully be made between a characteristic energy-loss structure and a characteristic *excess* energy-loss structure.

Let us consider a violent ion-atom collision in three steps, which are extensions of Russek's description⁴:

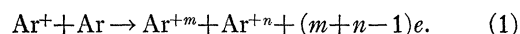
(1) As the two particles approach and recede, the energy levels interact and electrons undergo transitions. Every collision in a data set (at the same energy and angle) does not result in the same inelastic energy, and there is a distribution curve for inelastic energies. There is structure to this distribution which both in theory⁵ and experiment⁸ depends on the particular ion-atom combination. Our model is concerned with determining these distributions by analysis of the data.

(2) As the particles separate this inelastic energy must be distributed to the two particles. Our model is here concerned with the correlation between the energy received by one particle and that received by the other. Definite statements may be made about the portion of inelastic energy received by individual particles.

(3) Finally, after separation the excited atoms lose electrons. Our data analysis indicates that these electrons are in two categories: First, there may be (perhaps) one fast electron per atom emitted whose kinetic energy represents a certain sizeable fraction of the inelastic energy loss. This is consistent with the prediction by Fano and Lichten.⁵ Second, consistent with the theory by Russek,⁴ there is a statistical distribution of the remaining available energy among the other electrons with certain ionization probabilities.

2. DEFINITIONS

Certain quantities defined and measured in the preceding paper are listed for reference. Closely related quantities introduced in the present paper are also defined. Still other quantities are to be defined as needed throughout the text. The reaction under study is



m	The state of ionization of the scattered incident particle.
n	The state of ionization of the recoiling target particle.
i	The state of ionization of either particle after collision.
T_0	Incident-particle kinetic energy.
θ	Scattering angle of the scattered incident particle.
ϕ	Scattering angle of the recoiling target particle.
β	The sum $\theta + \phi$.
"data set"	The set of data obtained for all reactions wherein the T_0 and θ are held constant.
Q	Inelastic energy loss, general term referring to both particles and the collision as a whole.
\bar{Q}	The average inelastic energy loss associated with a given data set.
\bar{Q}_{mn}	The average (or most probable) inelastic energy loss associated with the (m,n) reaction within a given data set.
\bar{p}_{mn}	A differential quantity which is a measure of the probability of a particular (m,n) reaction versus Q within a data set. Its peak value is \bar{p}_{mn} .
\bar{p}_{mn}	The relative probability of the (m,n) reaction among all reactions in a given data set.

⁵ U. Fano and W. L. Lichten, *Phys. Rev. Letters* **14**, 627 (1965).

⁶ V. V. Afrosimov, Yu. S. Gordeev, M. N. Panov, and N. V. Fedorenko, *Zh. Tekhn. Fiz.* **34**, 1613, 1624, 1637 (1964) [English transl.: *Soviet Phys.—Tech. Phys.* **9**, 1248, 1256, 1265 (1965)].

⁷ M. Ya. Amusia, *Phys. Letters* **14**, 36 (1965).

⁸ V. V. Afrosimov, Yu. S. Gordeev, M. N. Panov, and N. V. Fedorenko, *JETP Pis'ma v Redaktsiyu* **2**, 253 (1965) [English transl.: *JETP Letters* **2**, 185 (1965)].

- E, E', E'' General term for the inelastic energy transferred to one of the particles. When necessary to make a distinction, a single prime refers to the scattered incident particle and a double prime refers to the recoiling target particle.
- \bar{E} The average (or most likely) value of E associated with one particle within a given data set.
- \bar{E}_i Within a given data set the average (or most likely) energy received by that subset of particles which are subsequently found to be in ionization state i .
- P_i The relative probability of ionization state i subsequently appearing in a particle which has received a specified inelastic energy E .
- \bar{P}_i The relative probability of a particle being in ionization state i after collision, when considering a given data set. Thus \bar{P}_i is an average value of $P_i(E)$ when there is a distribution of values E in a given data set. When considering measured values \bar{P}_i is a function of the average energy \bar{Q} in the data set.

3. DISTRIBUTIONS IN Q

As outlined in the Introduction, it is the thesis of the present paper that the $\text{Ar}^+ - \text{Ar}$ collision phenomena can be explained by a suitable distribution of the inelastic energy among all the collisions in a data set. The nature of this distribution is not known in advance, and several possible distributions in Q will be considered in turn. Data analysis will suggest rejection of certain of these possibilities. Attention is then directed to a distribution which will be developed here and compared with experiment.

a. Narrow Distribution in Q

Suppose there were a single value of Q for all collisions in a given data set. The consequence would be that all \bar{Q}_{mn} values within that set would be the same. This is overwhelmingly rejected by the data.^{1,2,6} There cannot be a single narrow Q value.

b. Characteristic Excess Energy Losses

The suggestion has been made^{6,7} that there are characteristic *excess* energy losses R^* in these $\text{Ar}^+ - \text{Ar}$ collisions, where

$$R^* = \bar{Q}_{mn} - U_{mn}. \quad (2)$$

Here U_{mn} is the deficit in spectroscopic ionization energies in the reaction of Eq. (1). Experiments by Afrosimov *et al.*^{6,8} suggested that R^* is independent of m, n, T_0 , and θ . They examine, particularly, an inter-

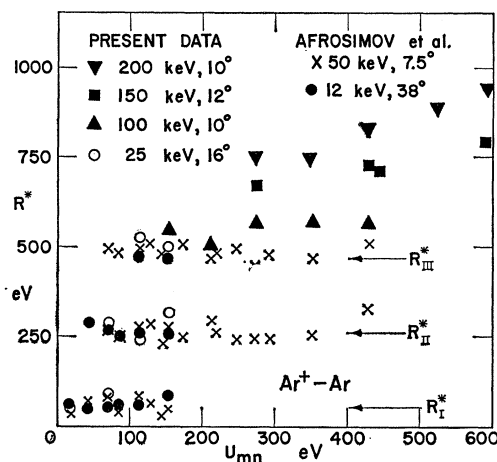


FIG. 1. Values of excess inelastic energy loss R^* are plotted versus U_{mn} , which is the spectroscopic energy deficit, for several data sets. These data are for $\text{Ar}^+ - \text{Ar}$ collisions.

esting region (shown also in Fig. 4 of the preceding paper¹) where there is a triple-structure to the Q values and obtain three characteristic excess energy values, R^*_{I} , R^*_{II} , and R^*_{III} for the successive peaks. They considered these three values to characterize the $\text{Ar}^+ - \text{Ar}$ collision.⁶

To examine the R^* concept a number of representative data sets are shown in Fig. 1, which plots R^* versus U_{mn} . Two data sets by Afrosimov *et al.*,⁶ and one of the present data sets¹ (25 keV, 16°) were taken in the triple-peak region. For these three data sets the values are indeed clustered around three levels R^* as indicated in the figure. However, for the more violent collisions, extending up to 200 keV, 10°, the data depart widely from R^*_{III} by amount which are far in excess of the experimental error. The data move up continuously, and there is no R^*_{IV} found.

A related corollary is that the energy \bar{Q}_{mn} associated with a particular (m, n) reaction is not a constant. This is shown by the vertical range of data points of Fig. 1, but shown better by Fig. 7 of the preceding paper¹ which plots \bar{Q}_{mn} versus \bar{Q} . Thus experiment shows that particular reactions do not have fixed values of inelastic energy loss, whether or not the values U_{mn} are subtracted.

As a model, the R^* concept has a certain usefulness in that it permits prediction of \bar{Q}_{mn} values in $\text{Ar}^+ - \text{Ar}$ collisions within a limited region. However, this concept does not correctly predict \bar{Q}_{mn} values outside this region, does not predict the relative abundances \bar{p}_{mn} , does not explain the peculiar kind of (m, n) correlations⁸ seen in the middle peak in the triple-peak region, and does not explain why the middle peak is found precisely midway between the outer two. Characteristic excess energy losses are not a *necessary* interpretation of the data. The present paper develops an alternative model which is free of the above limitations.

c. Broad Distribution in Q

A third possibility is that there may be broad distribution in Q values transferred during the collision and that each atom gets half of the transferred energy. This was the basis of the model presented in our first letter,² where it was seen that such a model could account quantitatively for the several \bar{Q}_{mn} values in each data set. However, if one carries out the development in detail along the lines already suggested² one finds that the relative abundances \bar{p}_{mn} are not predicted correctly. In fact, if each atom received half the energy, then there would be a kind of correlation in the \bar{p}_{mn} values. Low values of m would go with low values of n , etc. and this is not found.^{1,2} The model is not correct in assuming that each atom gets half the energy in a given collision.

d. Distribution Used in the Present Model

Although rather similar to the above, the distribution we consider next has an important distinction: It is assumed that there is no correlation between the energy received by one atom and the energy received by the other atom in the same collision. The starting point is the distribution in energy received by each atom individually.

Let E' be the inelastic energy received by the scattered incident particle, and let \bar{E} be its average value among such atoms in a given data set. A Gaussian distribution h' given by

$$h' = \Delta N' / \Delta E' = \exp[-(E' - \bar{E})^2 / a^2] \quad (3)$$

is assumed for the number $\Delta N'$ of such atoms in the range $\Delta E'$. The half-width a at $1/e$ height will be adjusted to fit the data. A constant having the dimensions of reciprocal energy is omitted from Eq. (3), and such constants are omitted for all distributions in this paper. The distribution is shown in Fig. 2(a). A similar distribution h'' , involving E'' , is assumed for the recoiling target atom.

The Q for each particular collision is

$$Q = E' + E'', \quad (4)$$

and in the present case where both particles are argon

$$\bar{E} = \bar{Q} / 2. \quad (5)$$

In the absence of correlation the two distributions are independent. The number $\Delta^2 N$ of events wherein the scattered incident particle receives energy between E' and $E' + \Delta E'$ and wherein the recoiling target particle receives energy between E'' and $E'' + \Delta E''$ is therefore the product $h'h''$. Thus,

$$\Delta^2 N(E', E'') = \exp[-(E' - \bar{E})^2 / a^2 - (E'' - \bar{E})^2 / a^2] \Delta E' \Delta E''. \quad (6)$$

It is rather surprising that E' and E'' can be considered independent of each other in this way. When E' is (say)

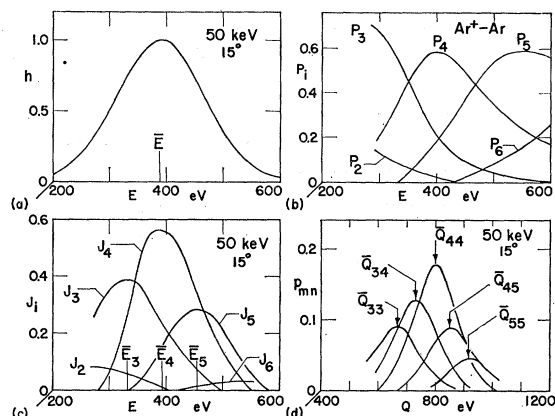


FIG. 2. (a) The distribution h in the inelastic energy E received per atom is plotted versus E . It is centered on the average energy \bar{E} for the 50 keV, 15° collision of Ar^+-Ar . (b) Curves of ionization probabilities P_i are plotted versus inelastic energy E per atom in Ar^+-Ar collisions. (c) These curves of J_i versus E represent products of the distribution h with the P_i curves. The energy at which the curve peaks is labeled \bar{E}_i . (d) The differential probability p_{mn} of the (m, n) event is plotted versus Q . The location of the peak of each curve predicts the corresponding average inelastic energy loss \bar{Q}_{mn} , and the height predicts \bar{p}_{mn} , which is the relative probability of the (m, n) event. These curves refer to 50 keV, 15° collisions of Ar^+-Ar .

higher than average, then E'' is just as likely to be above average as below average. The experimental data which requires this assumption is seen in Fig. 11 of the preceding paper,¹ which shows that the relative abundance of the charge states of one particle is almost independent of the charge state of the other particle.

The distribution of Eq. (6) is not directly observed because E' and E'' are not measured in the present experiment. However, $Q = E' + E''$ is a measured quantity, and the distribution in Q can readily be found by an integration of Eq. (6) holding $E' + E''$ constant. It is shown in the Appendix that

$$\Delta N / \Delta Q = \exp[-(Q - \bar{Q})^2 / 2a^2] \quad (7)$$

gives the distribution in Q . This distribution is $\sqrt{2}$ times wider than either of the distributions h' or h'' above. The remainder of this paper is concerned with the development of a model which uses the distributions of Eqs. (3)–(7).

4. MODEL FOR THE COLLISION

a. Description

Having received a given inelastic energy E , an atom loses electrons with certain statistical probabilities such that $P_i(E)$ is the probability of eventually losing i electrons. These probabilities, for various i , are plotted versus E in Fig. 2(b). This concept was introduced by Russek in his statistical-ionization theory.⁴

The $P_i(E)$ curves of Fig. 2(b) have the same general shape as the $\bar{P}_i(\bar{Q})$ data shown in Fig. 5 of the preceding paper, but they are not of the same height. A statistical distribution in E' and E'' has an averaging

effect which significantly lowers or "squashes" the data curves \bar{P}_i below the unaveraged P_i curves. A qualitative prediction of such a lowering appears in Russek's fourth paper⁴ although the large extent of the lowering was not realized.

Suppose that both the distribution h' and the $P_i(E)$ curves of Fig. 2(a) and 2(b) are known, postponing for a moment the discussion as to how these are obtained from the data. Here the primes may be dropped since the discussion may refer to either the group of scattered incident particles or the group of recoiling target particles, all within the same data set. The next step is to calculate the product $J_i(E)$ of the curve of Figs. 2(a) with a P_i curve of Fig. 2(b). Thus

$$J_i(E) = h(E)P_i(E), \quad (8)$$

as plotted in Fig. 2(c), is a measure of the number of (say) scattered incident atoms in a data set which receive energy between E and $E + \Delta E$ and which subsequently become i times ionized. The area under the J_i curves is proportional to the number of atoms among (say) the scattered incident particles which attain ionization state i . If one assumes that the several J_i curves of Fig. 2(c) have approximately the same half-widths (at $1/e$ height) then the peak height is a measure of the area. Let \bar{E}_i be the location in energy of the peak of the $J_i(E)$ curve. Then the measured \bar{P}_i are predictable by the peak heights $J_i(\bar{E}_i)$, except for normalization. Thus

$$\bar{P}_i = J_i(\bar{E}_i) / \sum_i J_i(\bar{E}_i). \quad (9)$$

The next steps are to predict the \bar{Q}_{mn} values and the relative abundances \bar{p}_{mn} from this model. The number $\Delta^2 N_{mn}$ of events wherein the scattered incident particle receives energy between E' and $E' + \Delta E'$ and subsequently becomes m times ionized, and wherein the recoiling target particle receives energy between E'' and $E'' + \Delta E''$ and subsequently becomes n -times ionized, is

$$\Delta^2 N_{mn}(E', E'') = J_m(E') J_n(E'') \Delta E' \Delta E''. \quad (10)$$

This equation may be integrated once under the restraint that $E' + E'' = Q = (\text{const})$, as shown in the Appendix. A Gaussian distribution of half-width b (at $1/e$ height) is there used to approximate $J_i(E)$ and the result of the integration is the distribution $p_{mn}(Q)$. This is the number ΔN_{mn} of (m, n) events which occur when the inelastic energy is between Q and $Q + \Delta Q$. Approximately,

$$p_{mn}(Q) = \Delta N_{mn} / \Delta Q = \bar{p}_{mn} \times \exp[-(Q - \bar{E}_m - \bar{E}_n)^2 / 2b^2], \quad (11)$$

as pictured in Fig. 2(d). The area under a p_{mn} curve is proportional to the number of (m, n) events in the data set. All these curves have the same half-width so that the peak height is a measure of this area. The peak heights have been normalized so that their heights \bar{p}_{mn} would total unity when summed over all (m, n) combinations. Thus \bar{p}_{mn} is comparable with the experimental

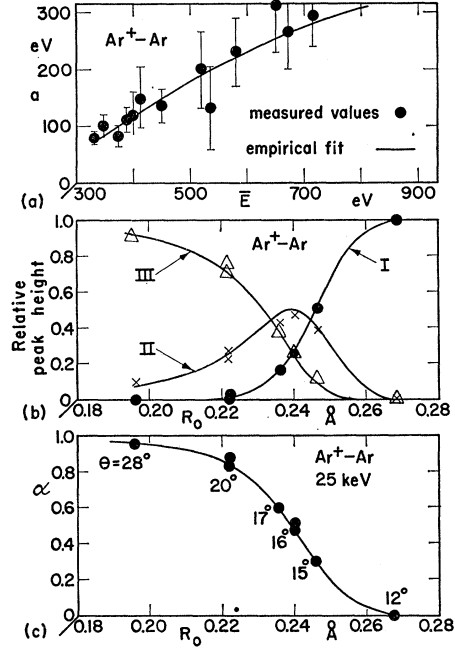


FIG. 3. (a) The half-widths a (at $1/e$ height) of the distribution in E are plotted versus average energy \bar{E} . The points are derived from measurements of natural linewidth, and the solid $a(\bar{E})$ curve shows values found empirically for best fit of the present model to the data. (b). This shows the relative heights of the three peaks in the triple-peak region plotted versus distance of closest approach R_0 . The solid lines are computed by the present model through the use of an adjustable parameter α . (c). Empirical values of the parameter α are plotted versus distance of closest approach R_0 . The values are fitted to 25-keV data taken at the angles θ specified. According to the present model, α is the fraction of the particles in a particular excitation state B after the collision.

quantity with the same notation measured in the preceding paper.¹ In the derivation of Eq. (11), as carried out in the Appendix, it is shown that

$$\bar{p}_{mn} = \bar{P}_m \bar{P}_n \quad (12)$$

in agreement with the empirical results^{1,3} of preceding work. Furthermore, Eq. (11) predicts that the $p_{mn}(Q)$ curves are peaked at a value \bar{Q}_{mn} where

$$\bar{Q}_{mn} = \bar{E}_m + \bar{E}_n. \quad (13)$$

This also may be directly checked against the data. When the two indices are equal, then

$$\bar{Q}_{ii} = 2\bar{E}_i, \quad (14)$$

where i equals either m or n , and the measured \bar{Q}_{mn} values, with Eq. (14) allow experimental determination of \bar{E}_m and \bar{E}_n within the framework of the model. Combining Eqs. (13) and (14) one obtains

$$\bar{Q}_{mn} = \frac{1}{2}(\bar{Q}_{mm} + \bar{Q}_{nn}) \quad (15)$$

which agrees with the data, empirically, as in Eq. (12) of the preceding paper.¹

It is possible to adjust the parameter a of this model to fit the data in detail. Figure 2(b) is a portion of a

TABLE I. For several typical data sets the measured values of \bar{P}_i , \bar{p}_{mn} , and \bar{Q}_{mn} are compared with values predicted by the present model.

T_0, θ, a	i	\bar{P}_i		m, n	\bar{p}_{mn}		\bar{Q}_{mn}, eV	
		Data	Model		Data	Model	Data	Model
50 keV, 15°, 109 eV	1	0.007		3,3	0.067	0.090	685±25	664
	2	0.057	0.051	3,5	0.061	0.062	814±18	787
	3	0.285	0.300	4,3	0.132	0.126	745±20	729
	4	0.427	0.420	4,4	0.181	0.176	805±16	794
	5	0.200	0.208	4,5	0.077	0.087	861±17	852
	6	0.025	0.019	5,5	0.030	0.043	915±25	910
				5,2	0.016	0.010		
				6,4	0.009	0.008		
				2,4	0.023	0.021		
				3,2	0.012	0.015		
100 keV, 10°, 146 eV	2	0.023	0.028	3,3	0.014	0.034	700±25	684
	3	0.145	0.183	4,3	0.053	0.068	790±25	768
	4	0.396	0.372	4,4	0.157	0.138	845±25	852
	5	0.352	0.346	4,5	0.144	0.129	925±25	918
	6	0.077	0.070	5,5	0.117	0.120	995±25	984
	7	0.007		3,6	0.018	0.013		
				5,3	0.059	0.064		
				6,6	0.006	0.005		
150 keV, 12°, 221 eV	2	0.008	0.023	4,4	0.040	0.053	950±40	860
	3	0.056	0.100	5,5	0.173	0.144	1150±40	1120
	4	0.220	0.230	6,4	0.068	0.054	1150±40	1120
	5	0.411	0.380	6,6	0.050	0.055	1410±50	1380
	6	0.257	0.235	5,4	0.096	0.088		
	7	0.057	0.036	7,4	0.014	0.008		
				3,6	0.019	0.024		
				6,5	0.112	0.089		
150 keV, 20°, 311 eV	3	0.018	0.026	5,5	0.046	0.067	1340±90	1320
	4	0.082	0.082	6,6	0.155	0.138	1660±100	1660
	5	0.259	0.258	7,7	0.041	0.048	2000±100	1950
	6	0.391	0.372	8,6	0.015	0.016		
	7	0.209	0.218	4,6	0.030	0.030		
	8	0.042	0.043	6,7	0.073	0.081		
				4,3	0.003	0.002		

universal set of curves for Ar^+-Ar , but Figs. 2(a), 2(c), and 2(d) have numerical values found to be appropriate to $T_0=50$ keV, $\theta=15^\circ$ data. The corresponding entry in Table I gives predicted \bar{Q}_{mn} and \bar{p}_{mn} values as read from Fig. 2(d) and compares these with the data. This fit is achieved by choosing the width a

in Eq. (3) to be 109 eV and by adjusting the heights of the $\bar{P}_i(E)$ curves as discussed below.

b. Choice of Width a

The measured natural linewidths δQ^N , as seen in Fig. 12(b) of the preceding paper, form a basis for choosing a . Thus δQ^N should correspond to the width $\sqrt{2}a$ of the distribution in Q , as in Eq. (7). The points in Fig. 12(b) of Ref. 1 may be transferred to Fig. 3(a) here, using $\bar{E}=\bar{Q}/2$ to change the abscissa and with $a=0.7\delta Q^N$. Because of the large error assigned to the measured linewidths, a is determined only approximately. There is leeway for an empirical adjustment. It is found that values of $a(\bar{E})$ indicated by the solid line in Fig. 3(a) give the best over-all agreement of our model with the data.⁹

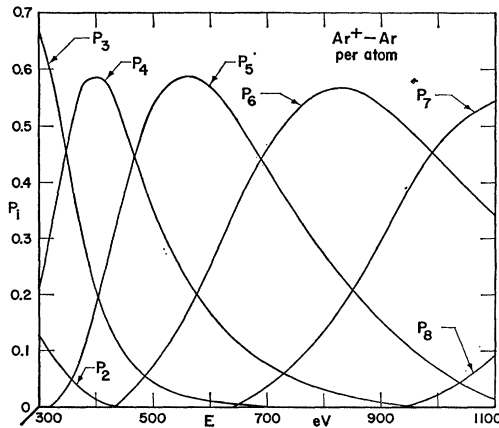


FIG. 4. Ionization probabilities P_i are plotted versus the energy E per atom in Ar^+-Ar collisions. These values are derived from the data with the use of the present model.

⁹ A detailed description of the empirical adjustment of a and the practical details of the unquashing process have been deposited as part of Document No. 8798 with the ADI Auxiliary Publications Project, Photoduplication Service, Library of Congress, Washington, D. C. 20036. A copy may be secured by citing the document number and by remitting \$2.50 for photoprints or \$1.75 for 35-mm microfilm. Advance payment is required. Make checks or money orders payable to: Chief, Photoduplication Service, Library of Congress.

c. Unsquashing the \bar{P}_i Curves

With the width $a(\bar{E})$ chosen it is possible to derive $P_i(E)$ curves from the $\bar{P}_i(\bar{Q})$ data. One uses the data to construct a set of curves which approximate Fig. 2(c) and then works backwards, within the framework of the model,⁹ to the $P_i(E)$ curves such as those in Fig. 2(b). This is done for all the data sets and a universal set of $P_i(E)$ curves is determined as in Fig. 4.

5. DISCUSSION

The $P_i(E)$ curves of Fig. 4 are believed to be unique. These curves, using the distribution width $a(\bar{E})$ shown in Fig. 3(a) suffice to predict the Ar⁺-Ar data.

a. Comparison with Data

The fact that all the data can be fitted within the present framework, and that one does not find inconsistencies in carrying out the above procedures, is the strongest indication of the usefulness of the model. Predicted values of \bar{p}_{mn} and \bar{Q}_{mn} are compared with their experimentally determined equivalents in Table I for 4 typical data sets. There is close prediction of the many data entries in this table. This agreement is achieved by selecting only the curve $a(\bar{E})$ for best fit.

The model does not predict quantities from first principles. Instead, it predicts relationships between measured quantities. In Table I the agreement between \bar{P}_i values as predicted and as measured is of minor significance, since such agreement is built into the model. However, other comparisons in the table are significant. There are three respects in which the success of the model may be judged at this stage:

(1) It predicts that $\bar{p}_{mn} = \bar{P}_m \bar{P}_n$. This is amply verified as seen by the entries in the table.

(2) The model determines a universal set of P_i curves from which the data may be developed. These curves have their counterpart in previous theoretical work.

(3) It demonstrates that there exists a distribution half-width a , consistent with measured linewidths, which predicts closely the relative order and spacing of the \bar{Q}_{mn} values.

Other predictions of the model are discussed below.

b. Comparison with Russek Theory

The set of curves shown in Fig. 4 are very similar in pattern to those predicted by Russek,⁴ except that the present P_i curves are higher and there are differences in the abscissas. There are three sets of curves by Russek to compare with Fig. 4: Set *A* is the "uniform ionization potential" curves as shown in Fig. 3 of Russek's first paper.⁴ Set *B* is the "self-consistent" curves described in Russek's fourth paper.⁴ (These were not plotted in a way as to be directly comparable with Fig. 4, but the desired curves for comparison can be extracted from the formulas and tables of that paper.)

Finally, there is set *C* which has been calculated by Russek and Meli.¹⁰ All these sets, *A* to *C*, differ in the way the inelastic energy is distributed among the electrons of the argon atom.

In Russek's first paper the P_i values of set *A* were found to agree very well with early data by Fuls *et al.*,¹¹ and later experiments by Pivovar *et al.*,¹² also agreed with set *A*. This agreement now appears to have been partly fortuitous. Early experimental difficulties¹¹ (probably too high a target gas pressure) gave \bar{P}_i values noticeably different from the present measurement.¹ More important, the large difference by reason of Q distributions between P_i as calculated and \bar{P}_i as measured had not hitherto been understood.

Russek's set of curves *B* and *C* represent successively better agreement with Fig. 4, but the heights of the several P_i peaks as calculated generally lie below those shown here.

c. Fast Electrons

There are three indirect reasons for suggesting for that one fast electron per atom is emitted in these collisions (above the triple peak region) in addition to the loss of a number of relatively slow electrons.

First, this supposition is consistent with Fig. 9 of the preceding paper,¹ in which the empirical curve of \bar{Q} versus $m + \bar{n} - 1$ has a discontinuity or gap in the triple-peak region. The upper branch of this curve is 300 to 400 V higher than would be expected from a continuation of the lower branch. Two fast electrons per collision (one per atom) is a possible explanation of this gap.

Second, this supposition is consistent with our first experiments in explanation of the triple structure,³ with its further explanation by Fano and Lichten,⁵ and with the detailed analysis of the triple-peak region to follow in Sec. 6.

Third, a comparison of Fig. 4 with Russek's curves not only strongly indicates that one fast electron is lost per atom but also gives a numerical estimate as to its kinetic energy. The abscissa E of Fig. 4 may be compared, at corresponding points, with the abscissa E_T of the calculated curves. For example, P_5 crosses P_6 at $E = 690$ eV on Fig. 4 and this same event occurs at $E_T = 705$ eV on the set of curves by Russek and Meli¹⁰ which are denoted as set *C*. This furnishes the point marked "5X6" on Fig. 5. To illustrate further, Fig. 4 shows P_4 to peak at $E = 400$ eV, whereas this peak occurs at $E_T = 340$ eV on the *C* curves. These values furnish the point marked "4" on Fig. 5. In this way corresponding points are compared and the results are

¹⁰ A. Russek and J. A. Meli (to be published). We thank Professor Russek and Meli for permission to incorporate their results here prior to publication.

¹¹ E. N. Fuls, P. R. Jones, F. P. Ziembra, and E. Everhart, *Phys. Rev.* **107**, 704 (1957).

¹² L. I. Pivovar, M. T. Novikov, and V. M. Tubayev, *Zh. Eksperim. i Teor. Fiz.* **46**, 471 (1964) [English transl.: *Soviet Phys.—JETP* **19**, 318 (1964)].

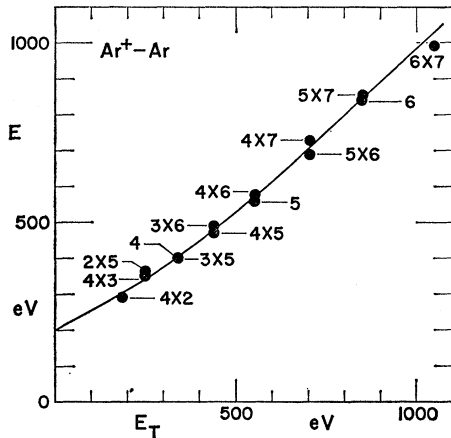


FIG. 5. Here the values of the energy E as derived here from the present measurement of Ar^+-Ar are compared with values of energy E_T as computed by Russek and Meli (Ref. 10) in their set C curves. Each point here refers to the corresponding locations of peaks or intersections as explained in the text. An empirical line connects the points.

connected by the empirical line on Fig. 5. This line, based on comparison with set C , extrapolates to $E=200$ eV at $E_T=0$. The same thing happens when set B is compared with Fig. 4; the extrapolated value of E is 175 eV in that case. There is here a strong indication that, above the triple-peak region, an amount of energy of the order of 200 eV per atom does not partake of the statistical distribution of inelastic energy within the atom. This energy could represent kinetic energy of a fast electron.

d. Linewidths

For reference, the several linewidths or distribution widths and their inter-relationships are summarized here:

- δQ^N The half-width at $1/e$ height of the distribution, as in Eq. (7), of the over-all inelastic energy loss Q (plotted versus Q).
- a The half-width at $1/e$ height of the distribution in E per atom plotted versus E . Here $a=0.7 \delta Q^N$ from Eqs. (3) and (7).
- b The half-width at $1/e$ height of a Gaussian which approximately fits the J_i distribution versus E of Fig. 2(c). Empirically, $b \approx 0.7 a$.
- δQ_{mn}^N The half-width at $1/e$ height of the p_{mn} distribution plotted versus Q , as pictured in Fig. 2(d). This equals $1.4b$, as shown in the Appendix.

A single equation displays these relationships:

$$\delta Q^N = 1.4a \approx 2b \approx 1.4\delta Q_{mn}^N. \quad (16)$$

It is seen in Fig. 3(a) that the values of δQ^N as derived from the data are consistent with the value of a necessary in the model. As seen in Eq. (16) the model predicts that the individual (m,n) reactions have a

natural half-width δQ_{mn}^N which is 0.7 the over-all natural half-width δQ^N . Unfortunately the (m,n) linewidth data of the preceding paper is not accurate enough to check this last prediction.

e. Possible Correlation

A fundamental assumption of the present model is that there is no correlation between the distribution in E received by one atom and that received by the other atom. This assumption is needed to write Eqs. (6) and (10) and leads to $\bar{p}_{mn} = \bar{P}_m \bar{P}_n$, which is Eq. (12). This prediction generally fits the data very well. There exists the possibility, however, that the data might be fitted even better by including a small amount of correlation in the model. Let us introduce a factor F defined by

$$F = \exp[-(E'+E''-\bar{Q})^2/c^2] = \exp[-(Q-\bar{Q})^2/c^2] \quad (17)$$

into Eq. (10). This factor would preferentially discriminate against events where $E'+E''$ is either much higher than or much lower than \bar{Q} . If the data are fit best with no correlation, then c will be infinite. If a small amount of correlation improves the fit to the data, then c will be finite though, presumably, considerably larger than a .

The factor F was incorporated into the theory and the data re-analyzed to find the best values of c . It was found that c was two to three times larger than a . Thus at 50 keV, 15° , the ratio c/a was 3.2 and at 150 keV, 12° the ratio c/a was 2.5. The factor F therefore represents only a very slight correlation and has little practical effect.

6. TRIPLE-PEAK REGION

The explanation of the triple peak as given in our recent letter³ is in accordance with the present model. Typical data are shown in Fig. 4 of the preceding paper.¹ In simple terms, one pictures the lowest Q peak as arising from a collision where each atom leaves in excitation state A . In the middle peak one atom is in state A and the other in state B , and in the highest Q peak each are in state B .

It should be emphasized that states A and B are not to be thought of as "characteristic" atomic levels, i.e., these states should not necessarily be expected whenever an argon atom makes a violent collision. Indeed, it is plausible that state B results from a vacancy in the L shell of the argon atom, where this vacancy occurs by a mechanism which may be peculiar to Ar^+-Ar interactions.⁵

These two states can now be incorporated into the present statistical model.

a. Doubly Peaked Distribution

Here it is assumed that the inelastic energy distribution received by a group of (say) scattered incident atoms has a double peak. One might picture the lower peak as representing excitations of the M shell to

varying degrees and the upper peak as other M -shell energies plus the energy needed to create a vacancy in the L shell. The relative heights of these two peaks are a critical function of T_0 and θ . This double peaked distribution would replace Fig. 2(a) and must be multiplied by values of $P_i(E)$ to reach a distribution analogous to Fig. 2(c) for each charge state i . The values of P_i given in Fig. 2(a) or Fig. 4 of this paper are suitable to the upper peak, but such curves are not now available for the lower peak. In fact, as discussed above it is likely that the curves of Fig. 4 include the effect, in both P_i heights and E , of a single fast electron of perhaps 200 eV, whereas the P_i curves suitable to the lower peak would not include this.

Analogous to Fig. 2(c) there would be instead a double peaked distribution $j_m(E') = \Delta N'_m / \Delta E'$ for the number $\Delta N'_m$ among that subset of scattered incident particles within the energy range $\Delta E'$ which subsequently become m times ionized. Let

$$j_m(E') = (1-\alpha)\bar{P}_m^A \exp[-(E' - \bar{E}_m^A)^2/b^2] + \alpha\bar{P}_m^B \exp[-(E' - \bar{E}_m^B)^2/b^2]. \quad (18)$$

Here α is the fraction in excitation state B (after collision) and $1-\alpha$ the fraction in state A . Here also \bar{P}_m^A is the probability of finding charge state m in peak A alone and \bar{P}_m^B refers to charge state m in peak B . In the above equation \bar{E}_m^A is the average (or most likely energy associated with finding charge state m in peak A , and \bar{E}_m^B is the same quantity referred to peak B . The half-width b of each distribution peak (at $1/e$ height) is chosen the same in order to avoid unessential algebraic complications.

Analogous to Eq. (18) there is a very similar expression for $j_n(E'')$ associated with finding charge state n among the set of recoil particles. In the absence of correlation, the differential number of (m,n) events, defined as in the text above Eq. (10), is the product.

$$\Delta^2 N_{mn}(E', E'') = j_m(E') j_n(E'') \Delta E' \Delta E''. \quad (19)$$

When this is multiplied out there are four terms on the right. However, if

$$\bar{E}_m^A + \bar{E}_n^B \approx \bar{E}_m^B + \bar{E}_n^A \approx 2\bar{E}_{mn}^{AB}, \quad (20)$$

which is a reasonable approximation, the two cross-product terms coalesce and Eq. (19) has then only three terms on the right.

Introducing $Q = E' + E''$ it is possible then to integrate Eq. (19) for each of the three terms following procedures rather similar to those shown in the Appendix. The resulting distribution in Q is

$$\begin{aligned} \Delta N_{mn} / \Delta Q = & (1-\alpha)^2 \bar{P}_m^A \bar{P}_n^A \\ & \times \exp[-(Q - \bar{E}_m^A - \bar{E}_n^A)^2 / 2b^2] \\ & + \alpha(1-\alpha) (\bar{P}_m^A \bar{P}_n^B + \bar{P}_m^B \bar{P}_n^A) \\ & \times \exp[-(Q - 2\bar{E}_{mn}^{AB})^2 / 2b^2] \\ & + \alpha^2 \bar{P}_m^B \bar{P}_n^B \\ & \times \exp[-(Q - \bar{E}_m^B - \bar{E}_n^B)^2 / 2b^2]. \quad (21) \end{aligned}$$

This triply peaked distribution is not unlike those shown in Fig. 4 of the preceding paper.¹ There are three centers, at $\bar{E}_m^A + \bar{E}_n^A$, at $2\bar{E}_{mn}^{AB}$, and at $\bar{E}_m^B + \bar{E}_n^B$. Equation (20) shows that the middle peak should be precisely midway between the outer two in apparent agreement with the data.

b. Correlation

Equation (21) shows that the first and third peaks should be uncorrelated with their \bar{p}_{mn} values given as in Eq. (12), but that the second or middle peak should show a particular kind of correlation which is predictable from the \bar{P}_i values measured for the two outer peaks. Thus, for the middle term of Eq. (21)

$$\bar{p}_{mn}^{AB} = \frac{1}{2} (\bar{P}_m^A \bar{P}_n^B + \bar{P}_m^B \bar{P}_n^A). \quad (22)$$

The factor $\frac{1}{2}$ replaces $\alpha(1-\alpha)$ because of normalization requirements, i.e., we are not concerned in Eq. (22) with the relative amplitudes of the three peaks, but rather with relative probability of the (m,n) reaction within the middle peak alone.

The pertinent data appear in the three sets of 25 keV, 16° data given in Table II of the preceding paper.¹ Except for notation, Eq. (22) is identical with Eq. (3) of our second letter,³ where the correlation data for the middle peak was found to agree with this expression.

The explanation of the triple structure by Fano and Lichten⁵ is entirely consistent with our analysis but treats another aspect of the problem. Drawing energy-level diagrams for Ar-Ar, they describe a mechanism for "promotion" of zero, one, or two L -shell electrons with subsequent emission of zero, one, or two fast electrons.¹³

c. Relative Peak Heights

Equation (21) may be summed over all (m,n) values to get an over-all distribution. One finds

$$\begin{aligned} \Delta N / \Delta Q = & (1-\alpha)^2 \exp[-(Q - \bar{Q}^A)^2 / 2a^2] \\ & + 2\alpha(1-\alpha) \exp[-(Q - \bar{Q}^{AB})^2 / 2a^2] \\ & + \alpha^2 \exp[-(Q - \bar{Q}^B)^2 / 2a^2], \quad (23) \end{aligned}$$

which is a triply peaked distribution centered on \bar{Q}^A , \bar{Q}^{AB} , and \bar{Q}^B which should describe the (T,T) curve in Fig. 4 of Ref. 1. The relationship between Eq. (23) and Eq. (21) is not exact. They are related in the same approximate way that Eq. (7) is related to Eq. (11).

¹³ Note added in proof. See also V. V. Afrosimov, Yu S. Gordeev, M. N. Panov, and N. V. Fedorenko, Zh. Tekhn. Fiz. 36, 123 (1966) [English transl.: Soviet Phys.—Tech. Phys. (to be published)]. This recent paper presents Ar⁺-Ar, Ne⁺-Ar, Ne⁺-Ne, and Kr⁺-Kr data within the pattern of their R^* interpretation. They ask how the occasional observation of the (1,4) event, for example, in the third peak can be consistent with a vacancy in the L shell of both atoms, since the incident particle, already singly ionized, would then have to lose at least one more electron. An answer is that because of charge transfer during the collision it is not possible to associate the one-electron deficiency with all the scattered incident particles.

Equation (23) predicts that the three (T,T) peaks should have amplitudes $(1-\alpha)^2$, $2\alpha(1-\alpha)$, and α^2 , respectively. This is readily compared with the data. The points in Fig. 3(b) show relative heights of the three peaks from several data runs and these are plotted versus distance of closest approach R_0 , which is thought to be the most appropriate abscissa. Thus the points at $R_0=0.24$ Å are obtained from the (T,T) contour in Fig. 4 of the preceding paper,¹ which shows 25 keV, 16° data. The solid lines in Fig. 3(b) show the nearest fit which can be achieved through the present model by making the best choice of the single parameter α at each R_0 value.

Data points taken by Afrosimov *et al.*,⁶ at 50 keV, $71\frac{1}{2}^\circ$ for the (2,3) reaction are shown by them plotted in a similar manner. In fact, we have been able to predict their data points fairly closely with our values of α and \bar{P}_i ; using Eq. (21) which predicts relative heights of specific m,n peaks.

The empirical values of $\alpha(R_0)$ needed to fit the data to the present model are shown in Fig. 3(c). This curve was obtained using 25-keV data at the angles noted on the figure, but is thought to be a universal curve when plotted versus R_0 . Figure 3(c) should be of considerable theoretical interest since it gives the relative population α of state B (and $1-\alpha$ of state A) as it depends upon distance of closest approach. Thus α may be related to the number and location of certain L -shell line crossings on the Ar^+-Ar energy-level diagram.

ACKNOWLEDGMENTS

We particularly wish to thank Professor Arnold Russek whose work provides the starting point of the present model and whose interest in this study is deeply appreciated. We thank Miss Marianne Melnick who carried out many of the calculations and data reductions.

APPENDIX

The steps connecting Eq. (6) to Eq. (7) are shown first: Let

$$Q = E' + E'', \quad \text{and} \quad R = E'' - E', \quad (\text{A1})$$

whence

$$\begin{aligned} E' &= \frac{1}{2}(Q - R), & E'' + E'^2 &= \frac{1}{2}(Q^2 + R^2), \\ E'' &= \frac{1}{2}(Q + R), & \Delta E' \Delta E'' &= \frac{1}{2} \Delta Q \Delta R. \end{aligned} \quad (\text{A2})$$

When this is substituted into Eq. (6) the result is

$$\begin{aligned} \Delta^2 N(Q, R) &= \frac{1}{2} \Delta Q \Delta R \\ &\times \exp[-(Q - 2\bar{E})^2/2a^2 - R^2/2a^2]. \end{aligned} \quad (\text{A3})$$

This may be integrated over all values of R with the result

$$\Delta N / \Delta Q = (\text{const}) \exp[-(Q - 2\bar{E})^2/2a^2]. \quad (\text{A4})$$

The multiplicative constant is dropped and $2\bar{E}$ is identified with \bar{Q} , as in Eq. (5). Thus Eq. (A4) is the same as Eq. (7).

The steps connecting Eqs. (10) to Eq. (11) are shown next: From Eq. (9) it is seen that the peaks of the J_i curves are proportional to \bar{P}_i . Although their shape is not Gaussian they may be so approximated. Thus $J_m(E')$, which appears in Eq. (10), is proportional to and has approximately the same shape as the function $\bar{P}_m \exp[-(E' - \bar{E}_m)^2/b^2]$, and $J_n(E'')$ may be approximated in a similar manner. Thus, in place of Eq. (10) one has, to a reasonably good approximation,

$$\begin{aligned} \Delta^2 N(E', E'') &= \bar{P}_m \bar{P}_n \exp[-(E' - \bar{E}_m)^2/b^2 \\ &\quad - (E'' - \bar{E}_n)^2/b^2] \Delta E' \Delta E'', \end{aligned} \quad (\text{A5})$$

where the constant of proportionality is omitted. When the substitutions indicated by Eqs. (A1) and (A2) are made the result is

$$\begin{aligned} \Delta^2 N(Q, R) &= \bar{P}_m \bar{P}_n \exp[-(Q - \bar{E}_m - \bar{E}_n)^2/2b^2 \\ &\quad - (R + \bar{E}_m - \bar{E}_n)^2/2b^2] \frac{1}{2} \Delta Q \Delta R. \end{aligned} \quad (\text{A6})$$

This may be integrated over all values of R and the resulting distribution in Q is

$$\Delta N / \Delta Q = \bar{P}_m \bar{P}_n \exp[-(Q - \bar{E}_m - \bar{E}_n)^2/2b^2], \quad (\text{A7})$$

where another multiplicative constant is not included. Equation (A7) is the same as Eq. (11) with the same normalization. The identification of $\bar{P}_m \bar{P}_n$ in Eq. (A7) with \bar{p}_{mn} in Eq. (11) leads to Eq. (12). Note that the half-width of the profile in Eq. (A7) is $1.4b$ and this should be the same as the natural (m,n) half-width δQ_{mn}^N .